Electronic supplementary information

Synergistically Enhanced Electronic Modulation in Trimetallic Cu-Co-Mo-Based Heterostructured Nanomaterials for Green H_2 Production via Efficient Alkaline Electrolysis

Apurba Borah,[a] Pooja,[a] Ravinder Pawar,[a] Gaddam Rajeshkhanna*[a]

[a]*Department of Chemistry, National Institute of Technology Warangal, Hanumakonda-506004, India.*

*E-mail: grkhanna@nitw.ac.in

1. Experimental section

1.1. Materials used. $Co(NO_3)_2.6H_2O$, $Cu(NO_3)_2.3H_2O$, $(NH_4)_6Mo_7O_{24}.4H_2O$, urea, NH_4F KOH pellets (85%), HCl (~35%) and acetone were purchased from FINAR of extrapure grade. $NaH_2PO_2.H_2O$ was purchased from Spectrochem and Na_2S from Burgoyne Burbidges & Co. of AR grade. RuO_2 and Pt/C (20 wt%) were purchased from Merck Sigma-Aldrich of AR grade. Commercially available nickel foam (NF) was purchased from Vritra Technologies. Double-deionized (DI) H_2O and ethanol were used for cleaning and synthesis.

1.2. Synthesis of electrocatalyst materials. 2×4 cm^2 of NF was cleaned by sonicating in an HCl solution (3 M) for 10 min to remove the oxidized surface layer followed by repeated washing with DI H_2O and acetone. The cleaned NF was dried for 1 h at 35 °C in a hot air oven. The dried NF was then placed inside a Teflon-lined stainless steel autoclave (50 mL capacity) containing a solution of DI H_2O (40 mL), where $Co(NO_3)_2.6H_2O$ (2 mmol), $Cu(NO_3)_2.3H_2O$ (1 mmol), $(NH_4)_6Mo_7O_{24}.4H_2O$ (0.6 mmol), urea (15 mmol) and NH_4F (4 mmol) were dissolved. The tightly closed autoclave was heated at 120 °C for 12 h in a hot air oven and cooled naturally to room temperature. Light brown colored material deposited NF was repeatedly washed with DI H_2O and ethanol followed by drying at 60 °C for 4 h. The obtained

material on NF was named CuCoMo-LDH. To convert the CuCoMo-LDH into the corresponding phosphide, CuCoMo-LDH and $NaH_2PO_2.H_2O$ were placed inside the tube of a tubular furnace with $NaH_2PO_2.H_2O$ (1 g) in the upstream position of the flowing N_2 gas. The tubular furnace was heated at a ramp rate of 3 °C min^{-1} up to 400 °C, and for 2 h at 400 °C with continuous N_2 gas flow. The obtained black-colored material deposited on NF was named CuCoMo-P. To get the corresponding sulfide of CuCoMo-LDH, Na_2S (10 mmol) was dissolved in DI H_2O (40 mL) and a 50 mL Teflon-lined stainless-steel autoclave was filled. CuCoMo-LDH was placed inside the Na_2S solution containing autoclave and heated at 120 °C for 6 h. After naturally cooling to room temperature, the black-colored material on NF (CuCoMo-S) was washed with DI H_2O and ethanol, followed by drying at 60 °C for 4 h.

Following a similar procedure as mentioned above, to get the monometallic Co-based electrocatalyst, a solution containing $Co(NO_3)_2.6H_2O$ (2 mmol), urea (15 mmol) and NH_4F (4 mmol) was used. The obtained NF-supported material was named $Co(OH)_2$. Similarly, a solution containing $Co(NO_3)_2.6H_2O$ (2 mmol), $Cu(NO_3)_2.3H_2O$ (1 mmol), urea (15 mmol) and NH_4F (4 mmol) was used to get the bimetallic material named CuCo-OH. Lastly, a solution containing $Co(NO_3)_2.6H_2O$ (2 mmol), $(NH_4)_6Mo_7O_{24}.4H_2O$ (0.6 mmol), urea (15 mmol) and NH_4F (4 mmol) was used to get the bimetallic material named CoMo-OH.

1.3. RuO_2 and Pt/C electrode fabrication. RuO_2 (15 mg) and Pt/C (20 wt% Pt content) (15 mg) were taken in two separate glass vials. A mixture of DI H_2O (480 µL), i-propyl alcohol (480 µL) and 5 wt% Nafion solution (40 µL) was added to the RuO_2 and Pt/C samples and sonicated for 30 min to get a homogeneous mixture. The catalyst inks were drop cast evenly on a 1×1 cm^2 NF separately and dried at 60 °C for 8 h. The amount deposited on NF in each case is ~9 mg cm^{-2}.

1.4. Characterization. Powder X-ray diffraction (PXRD) patterns were recorded by XPERT-PRO diffractometer system using Cu Kα radiation of λ = 1.54 Å. Fourier-transform

infrared (FT-IR) spectroscopy was conducted in the wavenumber window of 400 to 4000 cm^{-1} using BRUKER ALPHA II instrument. Thermo Fisher FEI-Quanta 250 FEG (FE-SEM) instrument was used to record field emission scanning electron microscopy (FE-SEM) images and energy-dispersive X-ray (EDX) spectra. High-resolution transmission electron microscopy (HR-TEM) imageries were recorded with the help of 200 kV Jeol/JEM 2100 instrument. Brunauer-Emmett-Teller (BET) analysis was done in Quantachrome® Autosorb iQ instrument. Surface elemental composition analysis was done by recording X-ray photoelectron spectroscopy (XPS) with the help of ULVAC PHI (VersaProbe III) instrument.

1.5. Electrochemical measurements. All the electrochemical measurements were performed using a BioLogic Science SP150e potentiostat. Oxygen evolution reaction (OER) and hydrogen evolution reaction (HER) studies were carried out in a conventional three-electrode system, and overall water splitting (OWS) studies were recorded using a two-electrode system. For the three-electrode systems, the Hg-HgO (1 M KOH) electrode, graphite rod, and 1 cm^2 area of the catalyst-loaded (~8 mg cm^{-2}) nickel foams (NFs) were used as the reference, counter, and working electrode, respectively. For two-electrode systems, two similar materials were used as anode and cathode as a symmetrical electrolyzer. The measured potentials against the Hg-HgO reference electrode were converted to the reversible hydrogen electrode (RHE) for better comparison with reported results using the equation:[1]

$$E_{RHE} = E_{Hg-HgO} + 0.059 \times pH + 0.098\ V \quad (1)$$

1 M KOH was used as the electrolyte solution in all cases (pH~14). Prior to electrochemical studies, all the working electrodes were activated by 100 continuous cycles of cyclic voltammetry (CV) at a scan rate of 50 mV s^{-1} to stabilize the electrocatalyst to have more accurate results. Linear sweep voltammetry (LSV) curves were recorded at a scan rate of 2 mV s^{-1} for OER, HER, and OWS without any iR-compensation to better understand the usability

of the electrodes in real applications. The overpotentials (η) calculation was done according to the equations:[2]

for HER, $\eta = E_{RHE} - 0\ V$ and (2)

for OER, $\eta = E_{RHE} - 1.23\ V$ (3)

The Tafel plots were derived from LSV curves to better understand the kinetics of OER and HER by using the following equation:[3,4]

$$\eta = a\log j + b \quad (4)$$

where a defines the Tafel slope, j defines the current density and b is the intercept on the overpotential axis. A faster reaction kinetics is accompanied by a smaller Tafel slope, whereas a slower reaction kinetics results in larger Tafel slope values.[3,4]

Exchange current densities (j_0) were calculated using Nyquist plots by the following equation:[5,6]

$$j_0 = \frac{RT}{nFR_{ct}} \quad (5)$$

where R defines the universal gas constant (8.314 J K^{-1} mol^{-1}), T is reaction temperature (298 K), n is the number of electrons transferred (n = 4 for OER, and n = 2 for HER), and R_{ct} is the exchange current density obtained from Nyquist plots.[5,6] Electrochemical impedance spectroscopy (EIS) was performed at 1.53 V for OER and -0.075 V for HER in the frequency range from 0.01 to 10^6 Hz to obtain the Nyquist plots.

The double-layer capacitances (C_{dl}) were measured using cyclic voltammetry curves in the non-faradaic region at scan rates ranging from 10 to 100 mV s^{-1}. The slopes obtained by plotting the difference in capacitive current densities vs. scan rates are equal to twice the C_{dl} values. The electrochemically active surface area (ECSA) was calculated from C_{dl} values following the formula:[1,2]

$$ECSA = \frac{C_{dl}}{C_s\ cm^{-2}_{ECSA}} \quad (6)$$

where C_s is the specific capacitance, which was assumed to be 0.04 mF cm^{-2} by considering the reported literature for a smooth metal surface.[1,2,7] Roughness factors (RFs) were also calculated from the ECSA values for the electrocatalysts using the following equation:[2]

$$RF = \frac{ECSA}{Geometric\ area\ of\ the\ electrode} \quad (7)$$

To evaluate the endurance of the electrocatalysts and fabricated electrolyzers, chronopotentiometry (CP) tests were conducted for the processes of OER, HER, and OWS at a current density of 50 mA cm^{-2} for a considerable duration of 100 h each. Furthermore, to assess the applicability of the electrocatalysts and electrolyzers, CP tests were carried out at even higher current densities of 100 and 200 mA cm^{-2}.

The turnover frequency (TOF), denoting the number of reactant molecules transformed into a product at each catalytically active site within a specified timeframe, has been computed in accordance with the ensuing equation:[4,8]

$$TOF = \frac{iN_A}{AFnG} \quad (8)$$

where *i* represents current (A), N_A defines the Avogadro number, *A* is the geometrical surface area of the electrode, *n* is the number of electrons transferred to the desired product, (*n* = 2 for H_2, and *n* = 4 for O_2), *F* defines Faraday's constant (96485 C mol^{-1}), and *G* represents the number of active sites.

The faradaic efficiency (FE) of the electrocatalyst for water electrolysis was calculated according to the following equations:[9]

$$\text{FE of } H_2 = \frac{\text{Experimental gas production in mL } (V_1)}{\text{Calculated gas production in mL } (V_2)} = {}^{V_1}/_{(2\ QV_m/4\ F)} \quad (9)$$

$$\text{FE of } O_2 = \frac{\text{Experimental gas production in mL } (V_3)}{\text{Calculated gas production in mL } (V_4)} = {}^{V_3}/_{(1\ QV_m/4\ F)} \quad (10)$$

where *Q* is the total charge passed through the electrodes, V_m is the molar volume of gas (22.4 L mol^{-1}, 293 K, 101 kPa), F is the Faraday constant (96485 C mol^{-1}), the number 4 defines 4

moles of electrons per mole of H_2O, the number 2 defines 2 moles of H_2 per mole of H_2O, and the number 1 defines 1 mole of O_2 per mole of H_2O.

1.6. Computational Details. In this study, density functional theory (DFT) calculations were carried out using the Vienna Ab initio Simulation Package (VASP).[10] Comparing the experimental results, it is clear that CuCoMo-P demonstrates superior electrocatalytic activity compared to CuCoMo-S and CuCoMo-LDH. Therefore, the theoretical investigation is focused exclusively on CuCoMo-P. The ratio of the atomic percentages in the supercell composition was determined using XPS analysis. As employed by Kresse and Joubert, projector augmented wave (PAW) potentials were used to describe the ion cores.[11,12] The Perdew-Burke-Ernzerhof (PBE) generalized gradient approximation (GGA) was applied to address electron exchange and correlation energies.[11,12] For structural relaxation in this investigation, the PBEsol approach was utilized.[13] Electron-core interactions were simulated using PAW pseudopotentials obtained from VASP.[10,14,15] These pseudo-potentials with a cutoff energy of 520 eV, represented the valence states of Co $3d^7\ 4s^2$, Cu $3d^{10}\ 4s^1$, Mo $4d^5\ 5s^1$, O $2s^2\ 2p^4$, P $3s^2\ 3p^3$, and for the H $1s^1$ were used. Geometry optimization was carried out until the energy variation was below 10^{-5} eV and the forces on each atom were less than 0.01 eV/Å. The Monkhorst-Pack sampling was conducted on the Brillouin zone with a Γ-centered grid of $2 \times 2 \times 1$.[16] The supercells were arranged such that the unit cell vectors *a* and *b* lay within the surface plane, while the vector *c* was oriented perpendicular to this plane. Following optimization via DFT calculations, the lattice vectors *a* and *b* for the catalyst were determined to be 6.58 and 9.93 Å, respectively. The unit cell vector *c* was fixed to 40 Å to ensure sufficient separation and avoid interactions between layers.

Detailed calculations were conducted to analyze the HER and OER pathways, employing the electrochemical analysis method developed by Nørskov and collaborators.[17] The hydrogen adsorption free energy (ΔG_{H^*}) was calculated using the equation:

$$\Delta G_{H^*} = \Delta E_{H^*} + \Delta ZPE - T\Delta S, \quad (11)$$

where, ΔE is the change of reaction energy, ΔZPE is the zero-point energy, and ΔS is the change in entropy.

In alkaline electrolytes, H_2O acts as the source of protons, defining the complete reaction pathway for OER as detailed below:

$$OH^- + * \rightarrow OH^* + e^- \quad \Delta G_1 \quad (12)$$

$$OH^* + OH^- \rightarrow O^* + H_2O + e^- \quad \Delta G_2 \quad (13)$$

$$O^* + OH^- \rightarrow OOH^* + e^- \quad \Delta G_3 \quad (14)$$

$$OOH^* + OH^- \rightarrow O_2 + H_2O + * + e^- \quad \Delta G_4 \quad (15)$$

where * signifies a potential adsorption site on the electrocatalyst. The adsorbed intermediates are represented as O*, OH*, and OOH*. For each elementary step, the Gibbs reaction free energy (ΔG) is determined by calculating the difference between the free energies of the initial and final states. This is expressed as:

$$\Delta G = \Delta E + \Delta ZPE - T\Delta S \quad (16)$$

where ΔE is the reaction energy of reactant and product moieties adsorbed on the catalyst surface derived from DFT analysis. The changes in zero-point energies (ΔZPE) and entropy (ΔS) due to the considered reactions are taken into account. The reaction free energies of equations (12) to (15) ($\Delta G_1, \Delta G_2, \Delta G_3,$ and ΔG_4) represent the reaction Gibbs free energies of the reactions. Furthermore, the Gibbs free energy corrections for gas-phase molecules were obtained from the NIST database**.**

2. Calculations of synthesis cost of electrocatalysts:

Cost of 2 mmol $Co(NO_3)_2.6H_2O$ = \$0.07

Cost of 1 mmol $Cu(NO_3)_2.3H_2O$ = \$0.006

Cost of 0.6 mmol $(NH_4)_6Mo_7O_{24}.4H_2O$ = \$0.11

Cost of 15 mmol Urea = \$0.008

Cost of 4 mmol NH_4F = \$0.003

Cost of 1 g $NaH_2PO_2.H_2O$= \$0.02

Cost of 10 mmol Na_2S = \$0.01

Cost of 40 mL DI H_2O = \$0.07

Cost of 8 cm^2 NF = \$0.143

The total cost of the CuCoMo-LDH electrocatalyst = \$0.41/8 cm^2 = \$0.051 cm^{-2}

The total cost of the CuCoMo-P electrocatalyst = \$0.43/8 cm^2 = \$0.053 cm^{-2}

The total cost of the CuCoMo-S electrocatalyst = \$0.42/8 cm^2 = \$0.052 cm^{-2}

The electricity consumption for the synthesis of CuCoMo-LDH is:

For the use of hot air oven-

Energy consumption = 1000 W × 12 h = 12000 W h = 12 kW h

Total electricity cost = 12 kW h × \$0.02/kW h = \$0.24

The electricity consumption for the synthesis of CuCoMo-P is:

For the use of hot air oven-

Energy consumption = 1000 W × 12 h = 12000 W h = 12 kW h

For the use of tubular furnace-

Energy consumption = 1500 W × 4.21 h = 6.32 kW h

Total electricity cost = (12 kW h × \$0.02/kW h) + (6.32 kW h × \$0.02/kW h) = \$0.37

The electricity consumption for the synthesis of CuCoMo-S is:

Total electricity cost = (12 kW h × \$0.02/kW h) + (6 kW h × \$0.02/kW h) = \$0.36

3. Cost of H_2 gas per kiloliter (kL)

Using the CuCoMo-P (±) electrolyzer:

Current applied = 500 mA = 0.5 A

The voltage required to reach 0.5 A = 2.5 V

Duration = 13 min = 0.22 h

Rate of H_2 production = 3.4 mL min^{-1}

The time needed for production of 1,000 L (1 kL) H_2 gas = 4902 h

Power consumption (H_2/kL) = 0.5 A × 2.5 V × 4902 h = 6127.5 W h = 6.1275 kW h

Cost of 1 kL H_2 gas = Power consumption × electricity bill

= 6.1275 kW h × \$0.02/kW h = \$0.12255

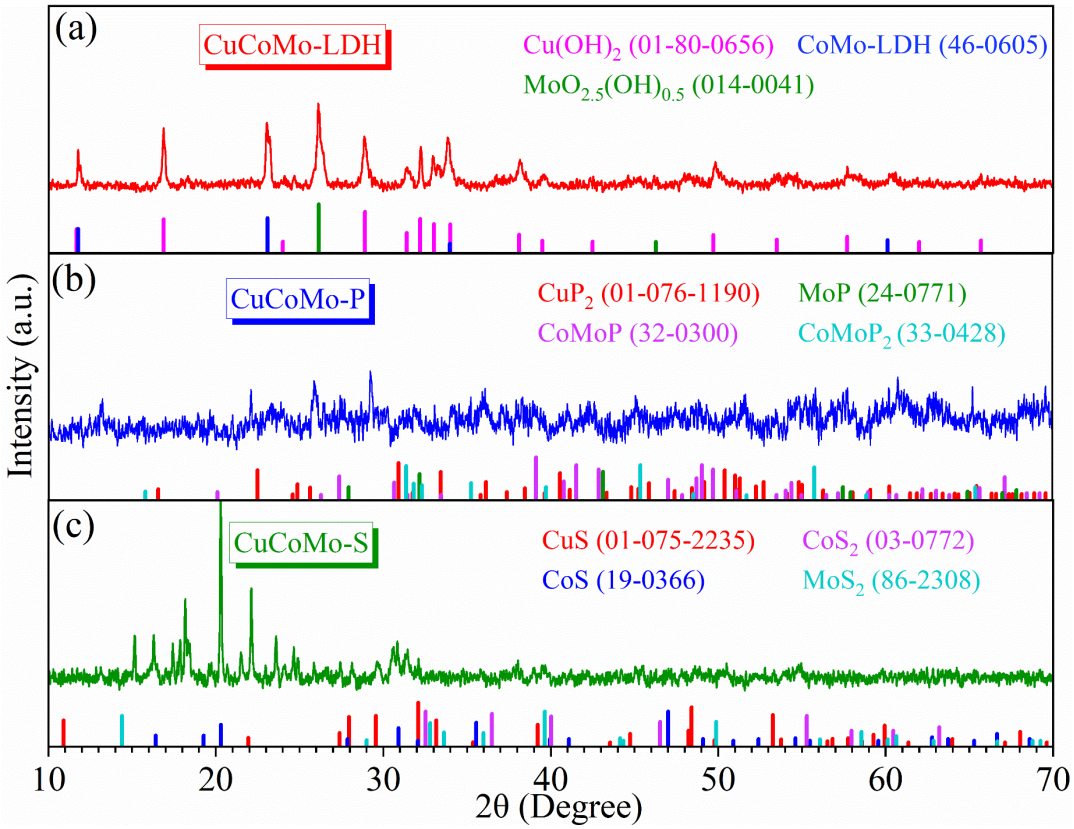

Fig. S1 PXRD patterns of (a) CuCoMo-LDH, (b) CuCoMo-P, and (c) CuCoMo-S.

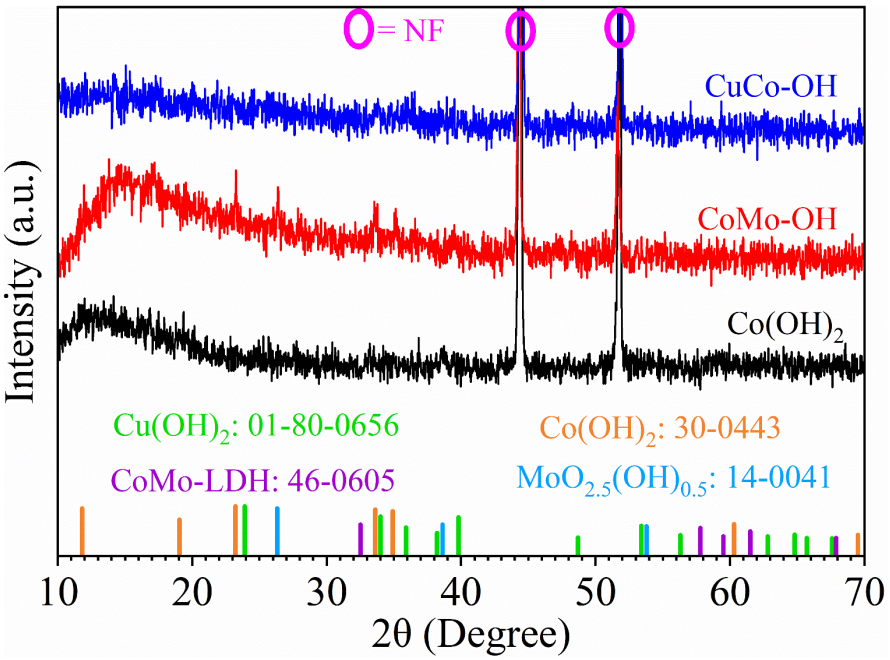

Fig. S2 PXRD patterns of the mono and bimetallic electrocatalyst materials.

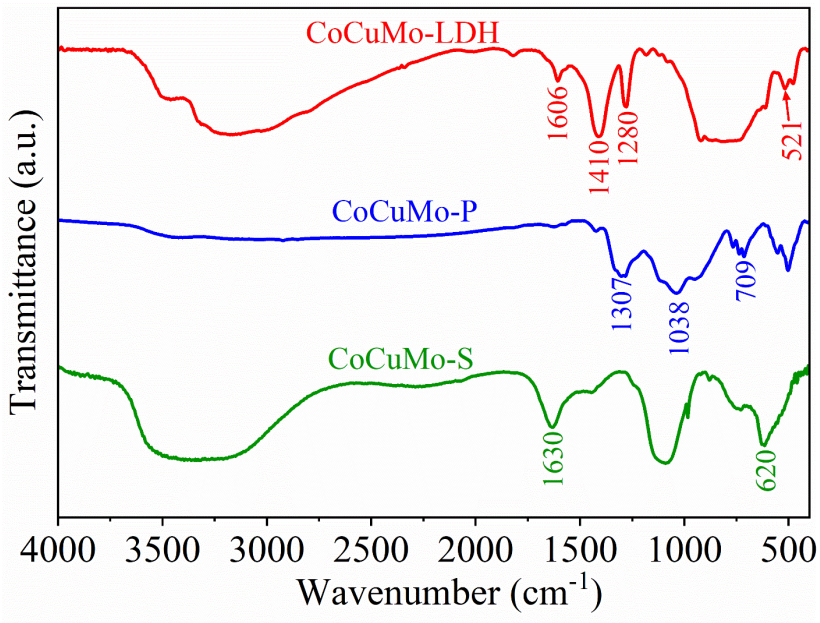

Fig. S3 FT-IR spectra of CuCoMo-LDH, CuCoMo-P and CuCoMo-S.

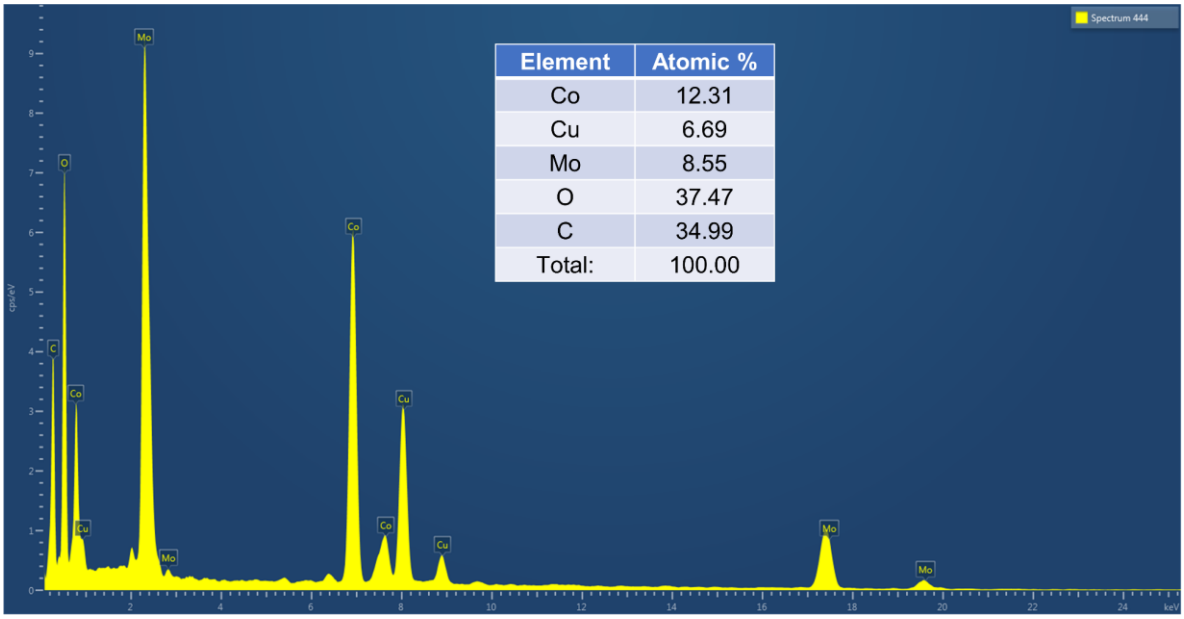

Fig. S4 EDX spectrum of CuCoMo-LDH.

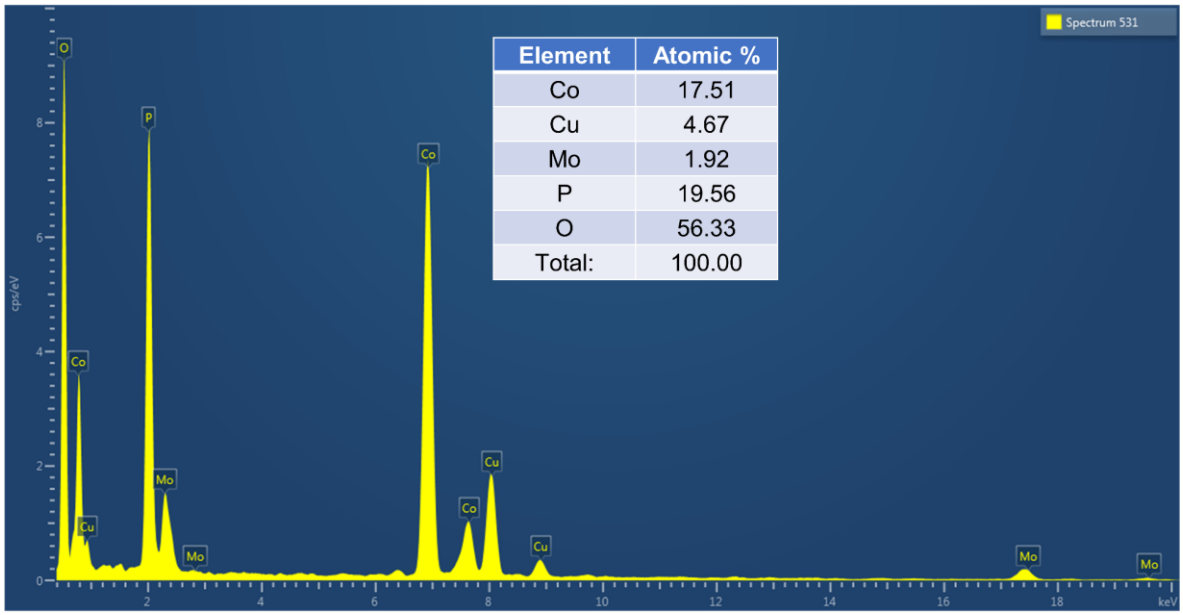

Fig. S5 EDX spectrum of CuCoMo-P.

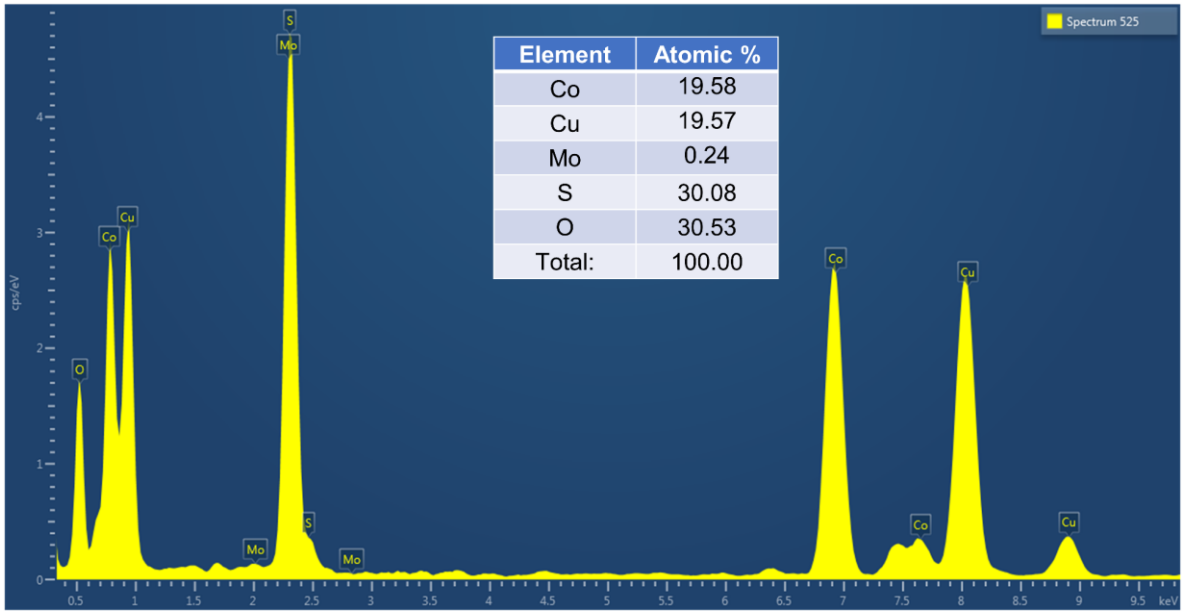

Fig. S6 EDX spectrum of CuCoMo-S.

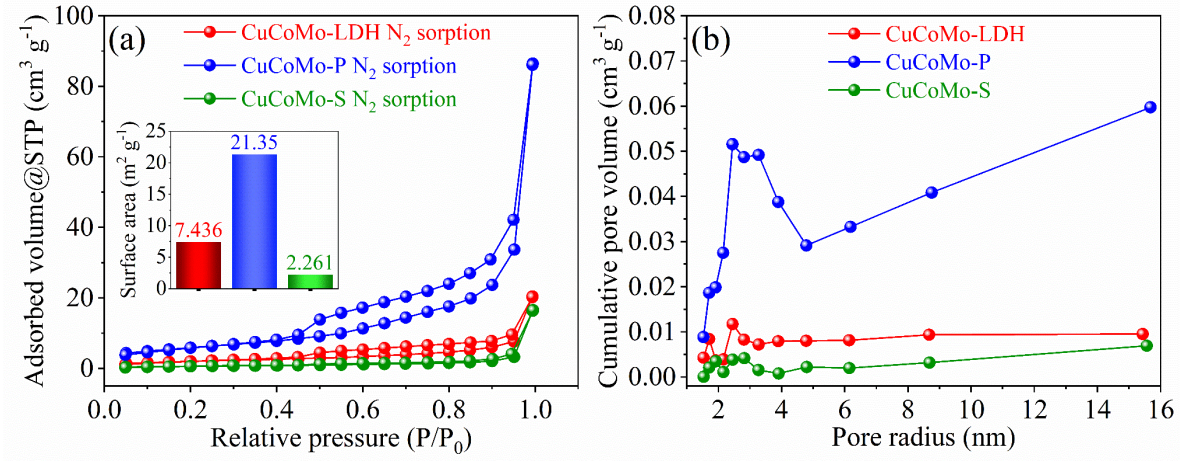

Fig. S7 (a) N_2 sorption BET isotherms, and (b) cumulative pore volume distribution plots.

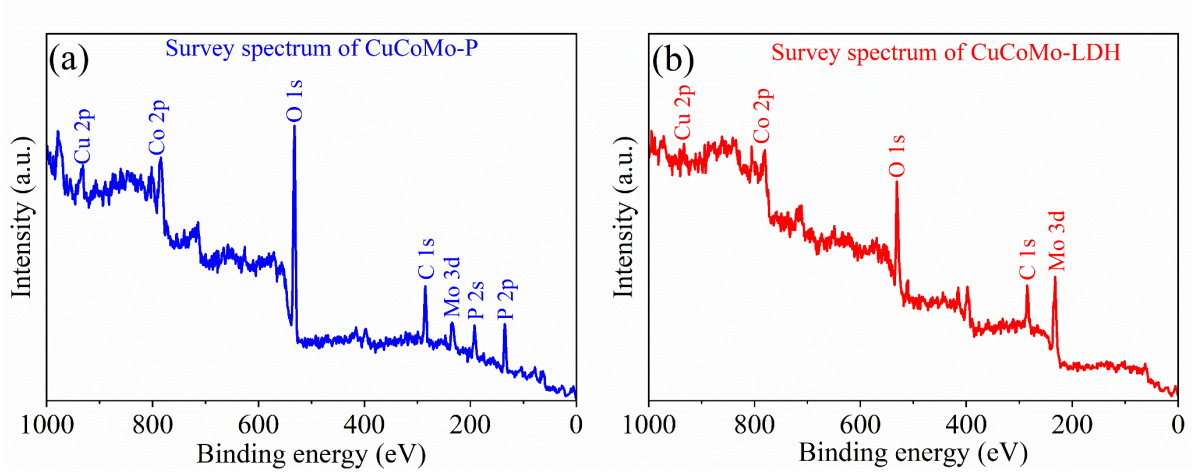

Fig. S8 XPS survey spectra of (a) CuCoMo-P, and (b) CuCoMo-LDH.

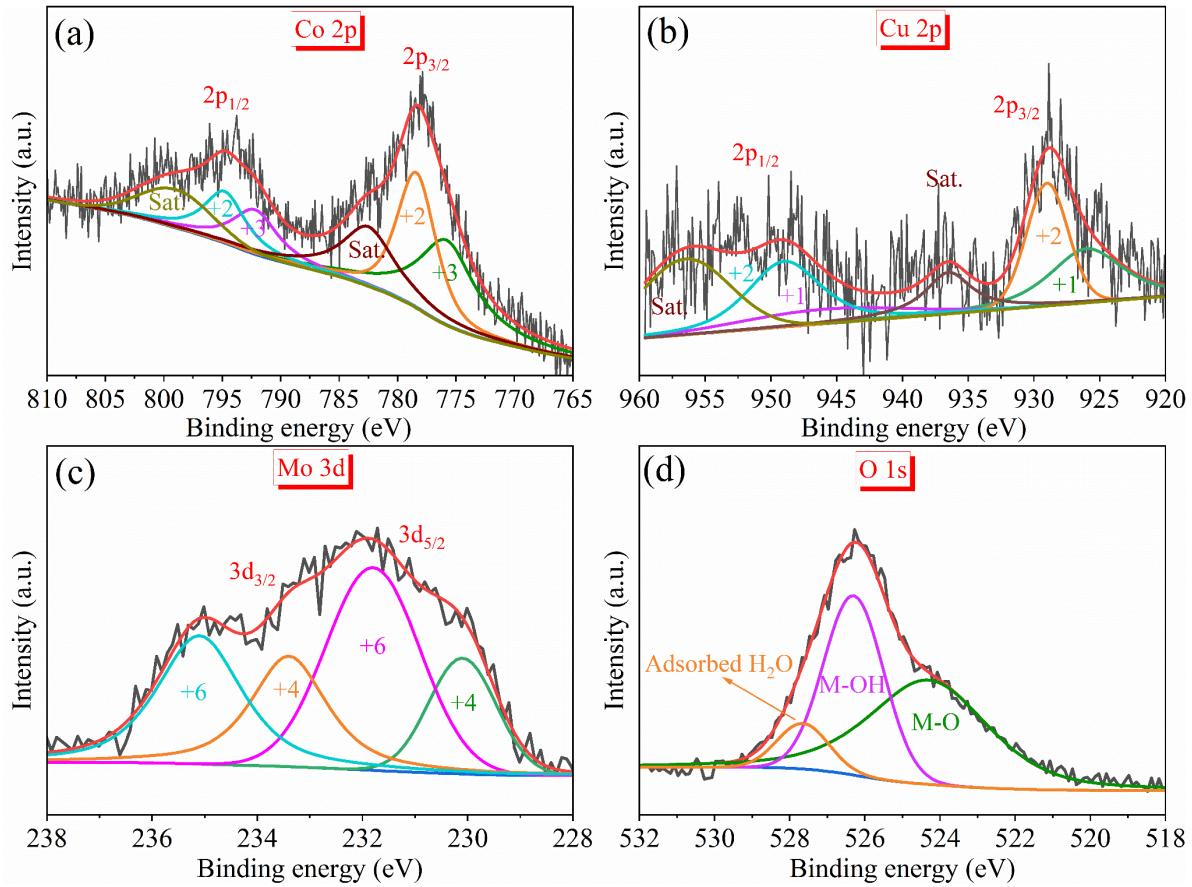

Fig. S9 XPS deconvoluted spectra of (a) Co 2p, (b) Cu 2p, (c) Mo 3d, and (d) O 1s of the CuCoMo-LDH.

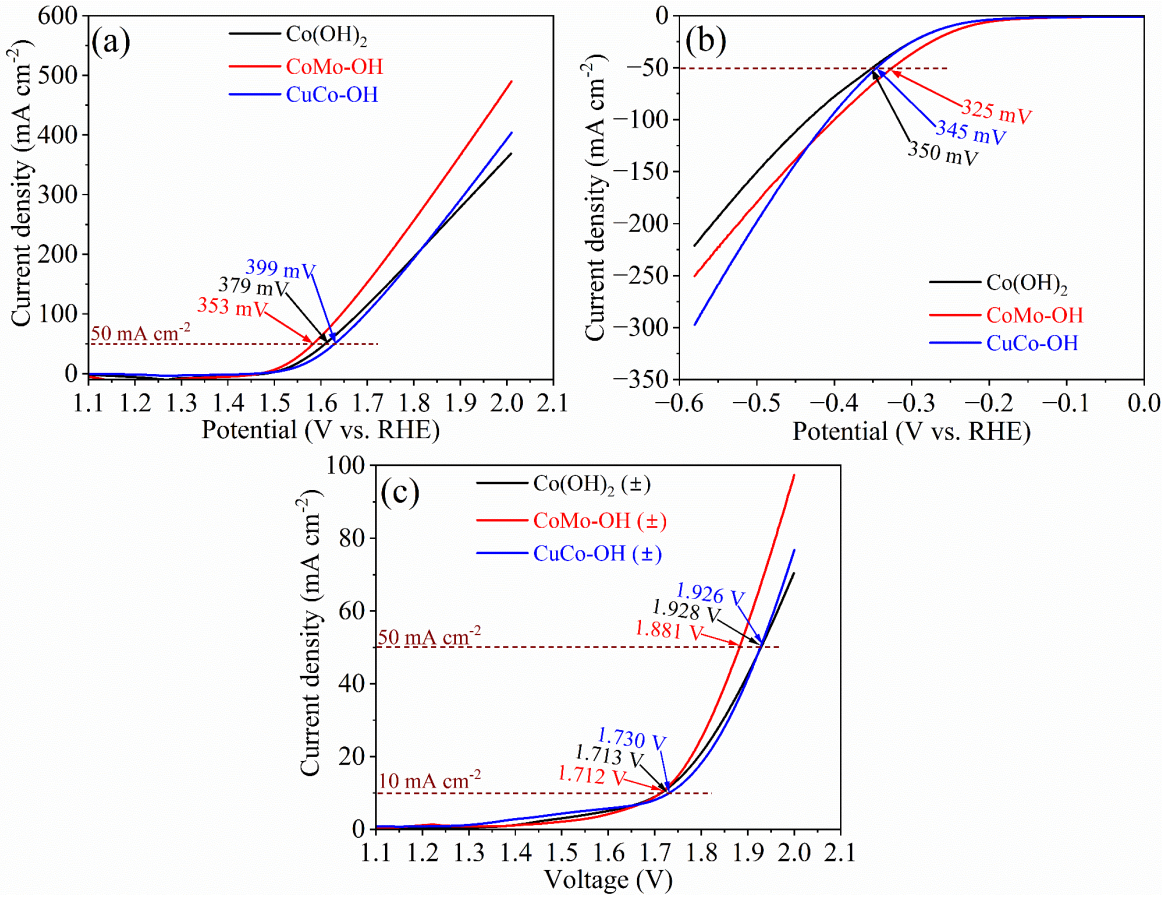

Fig. S10 LSV curves of $Co(OH)_2$, CoMo-OH and CuCo-OH for (a) OER, (b) HER, and (c) OWS.

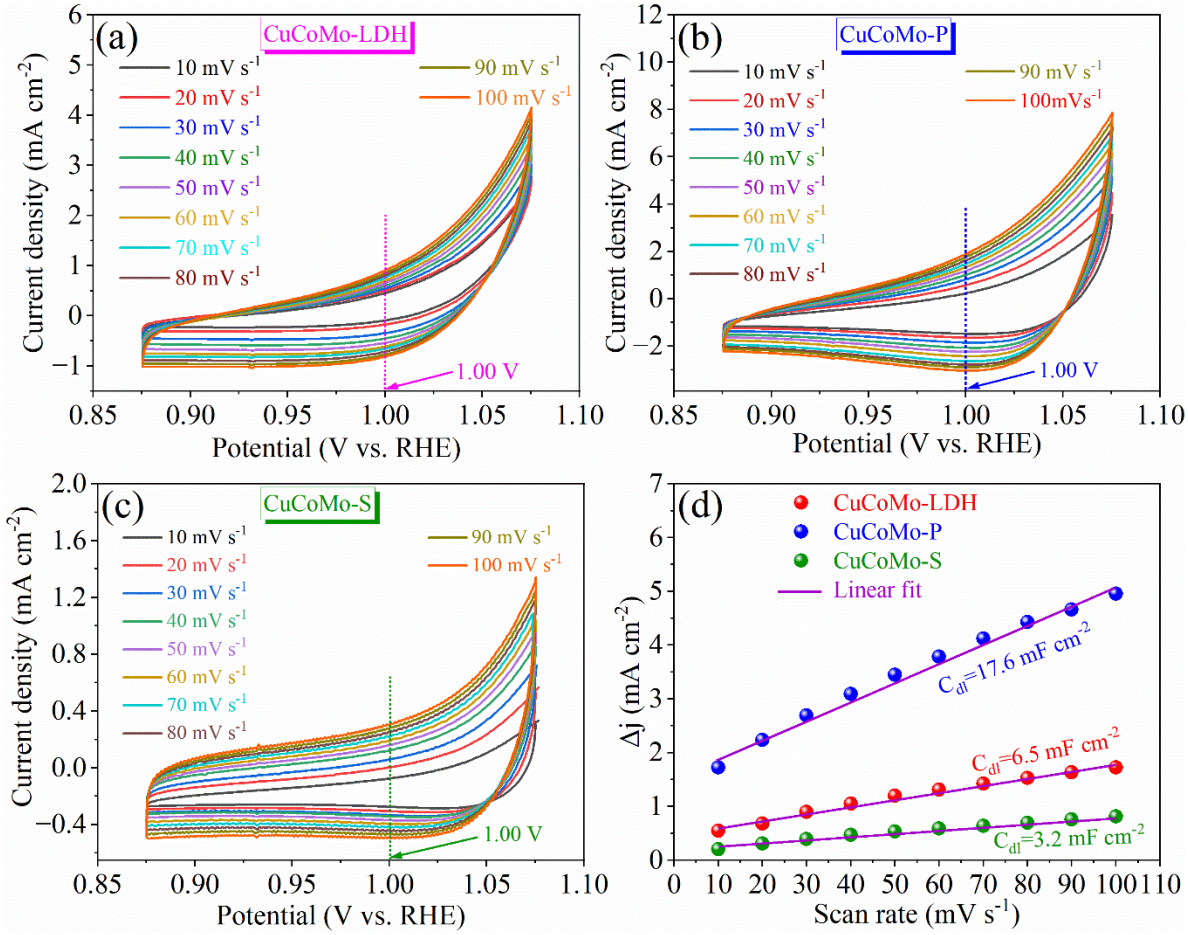

Fig. S11 Cyclic voltammograms at different scan rates of (a) CuCoMo-LDH, (b) CuCoMo-P, (c) CuCoMo-S, and (d) difference of anodic and cathodic current densities (Δj) vs. scan rate plots with C_{dl} values.

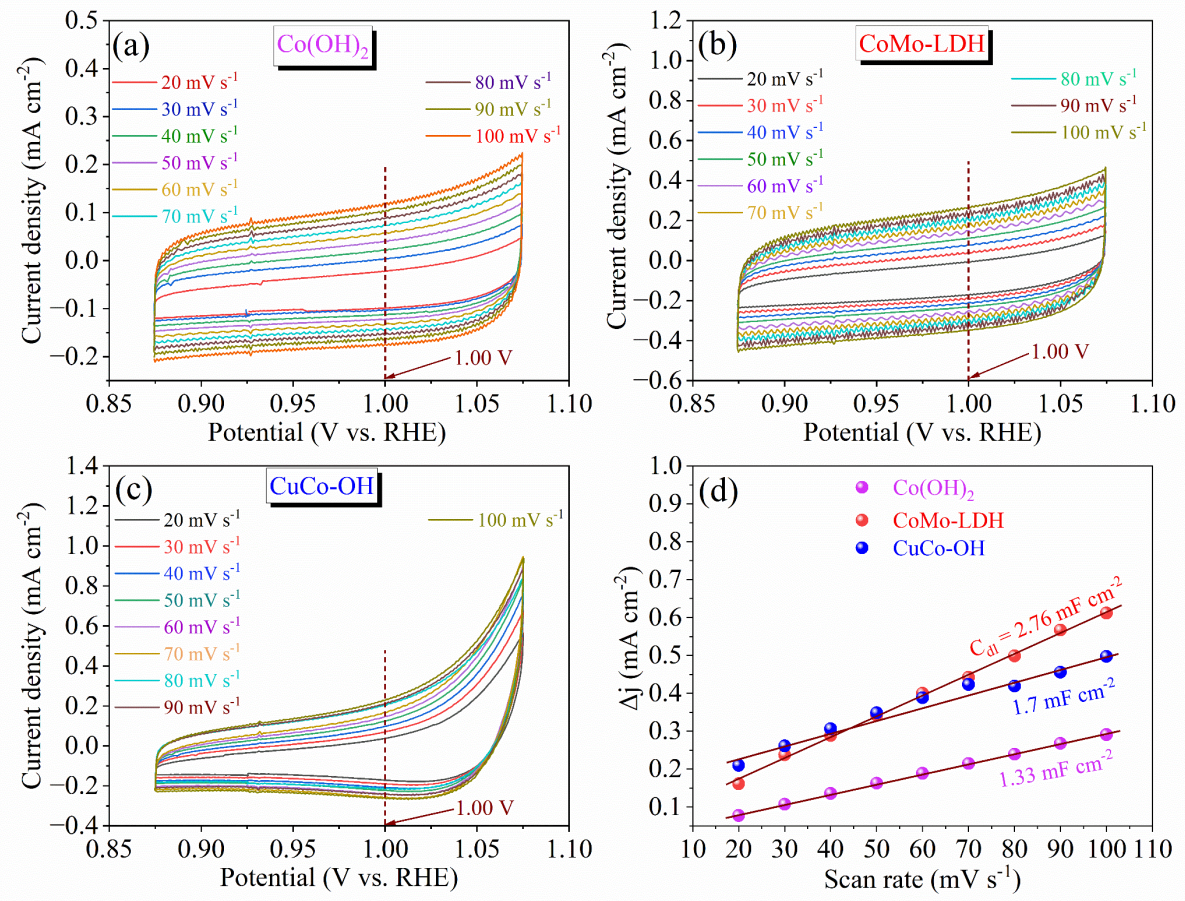

Fig. S12 Cyclic voltammograms at different scan rates of (a) $Co(OH)_2$, (b) CoMo-LDH, (c) CuCo-OH, and (d) difference of anodic and cathodic current densities (Δj) vs. scan rate plots with C_{dl} values.

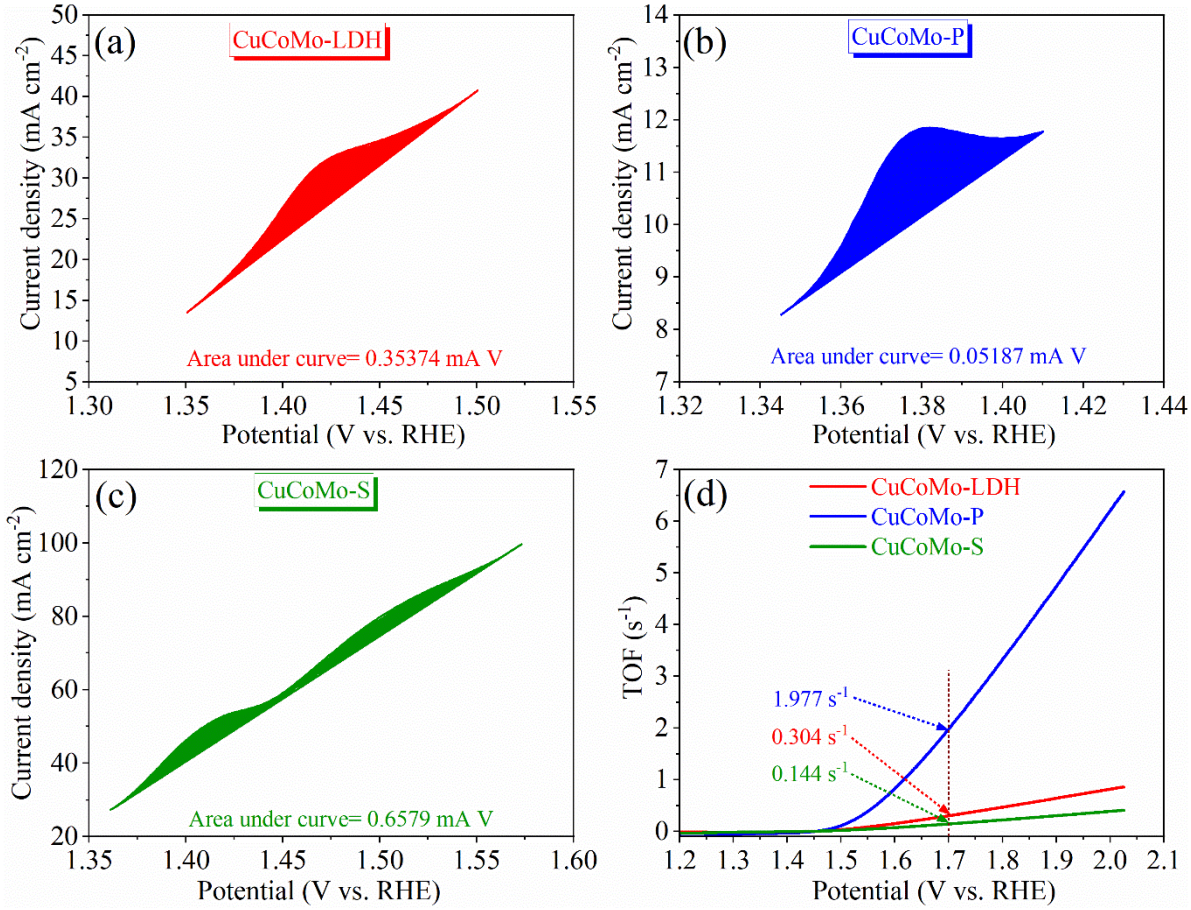

Fig. S13 Urea under the oxidation curve for (a) CuCoMo-LDH, (b) CuCoMo-P, (c) CuCoMo-S, and (d) TOF against the potential curve.

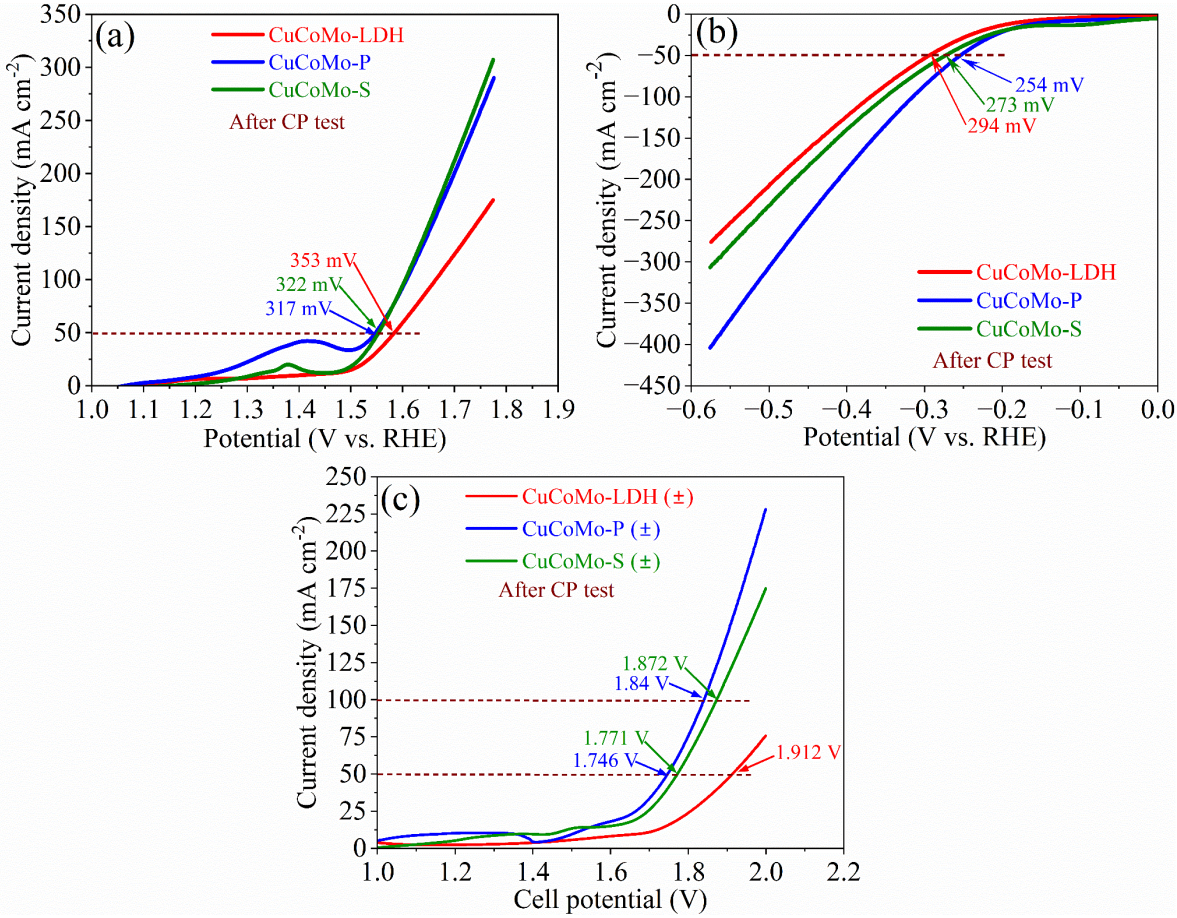

Fig. S14 LSV curves after chronopotentiometry test for (a) OER, (b) HER, and (c) OWS.

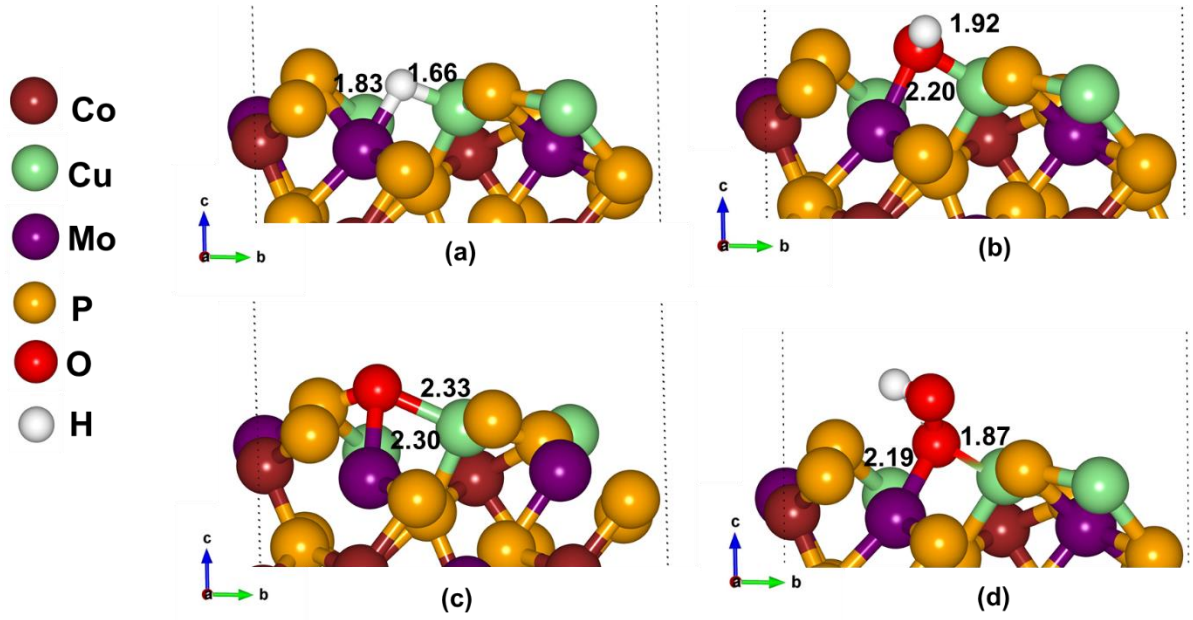

Fig. S15 Schematic representations are shown for intermediate structures of CuCoMo-P (a) with H for HER, (b) with OH, (c) with O, and (d) with OOH for OER, where the red, green, and blue arrows represent the *a*, *b*, and *c* vectors, respectively.

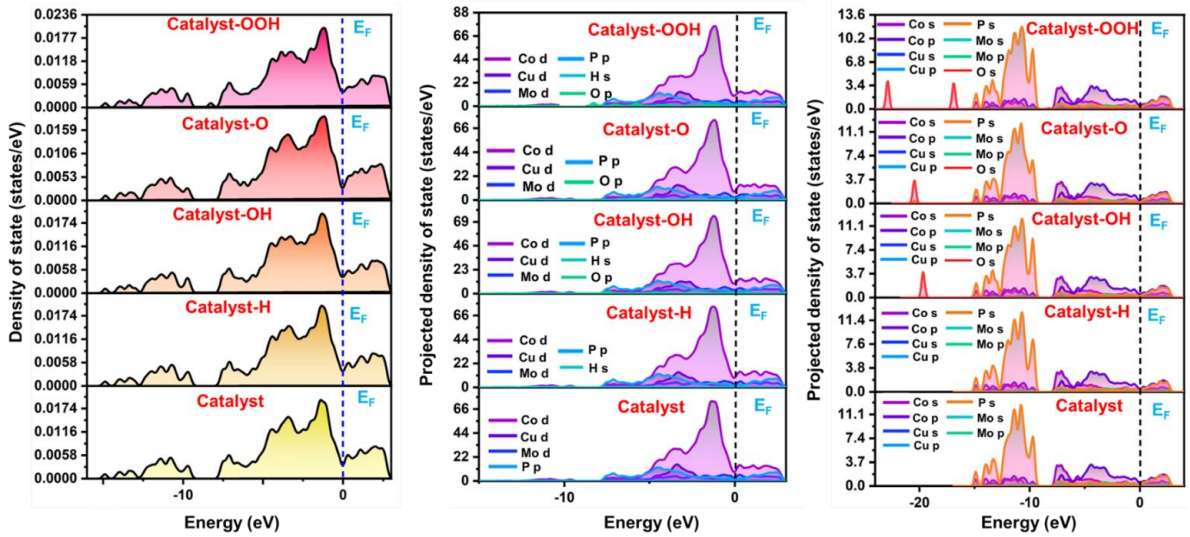

Fig. S16 The calculated electronic properties of CuCoMo-P and with intermediates involved in HER and OER. The terms catalyst, catalyst-H (H*), catalyst-OH (OH*), catalyst-O (O*), and catalyst-OOH (OOH*) refer to the catalyst alone, the catalyst with an H intermediate, the catalyst with an OH intermediate, the catalyst with an O intermediate, and the catalyst with an OOH intermediate, respectively.

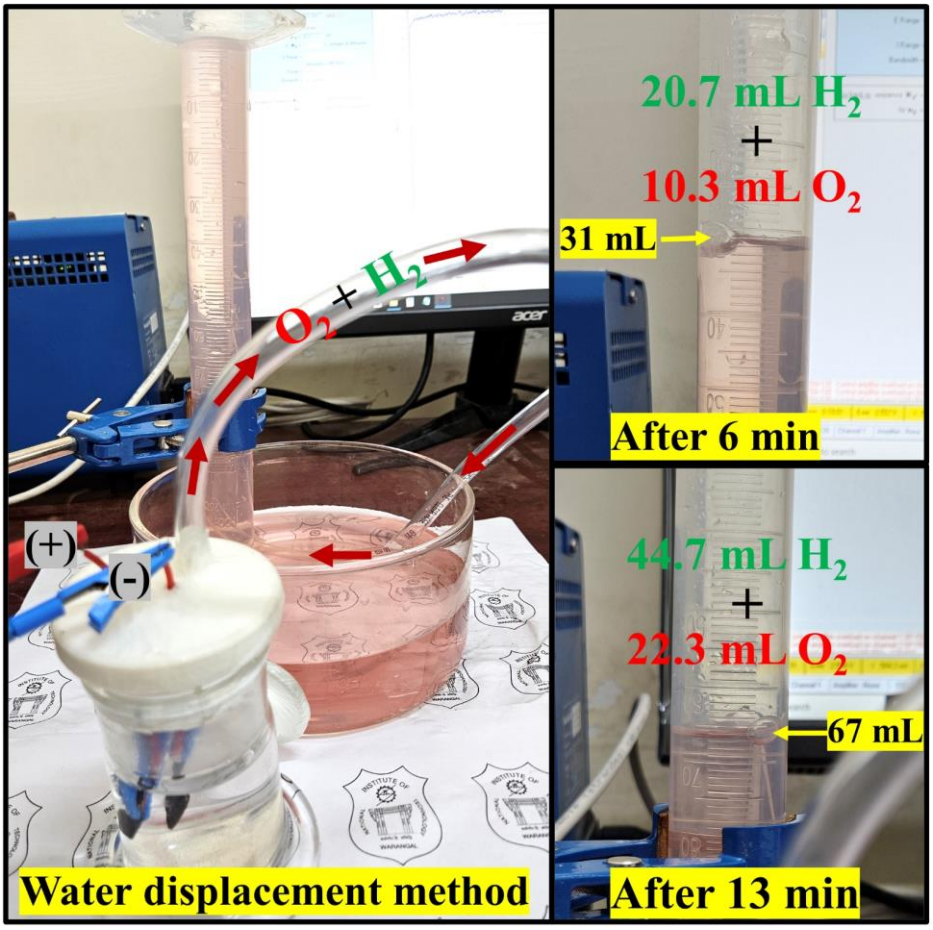

Fig. S17 Water displacement method for the measurement of H_2 and O_2 gas production by water electrolysis.

Table S1. Comparison of OER performance of the reported electrocatalysts with recent results.

Electrocatalyst	Electrolyte	Current density (mA cm^{-2})	Scan rate (mV s^{-1})	Overpotential (mV. vs RHE)	Ref.
CuCoMo-LDH	1 M KOH	10 50 100	2	264 307 363	This work
CuCoMo-P	1 M KOH	10 50 100	2	246 331 382	This work
CuCoMo-S	1 M KOH	10 50 100	2	241 311 375	This work
IrSAC-NiFe-LDH	1 M KOH	10	1	194	9
CoMoNiPi	1 M KOH	10	2	272	18
MoP/$CoMoP_2$@NPC	0.5 M H_2SO_4	10	5	261	19
MoP@NPC	0.5 M H_2SO_4	10	5	282	19
CoMoP2@NPC	0.5 M H_2SO_4	10	5	282	19
MoP/$CoMoP_2$@NPC	1 M KOH	10	5	284	19

Mo–$Co(OH)_2/Co_3O_4$/NF-800	1 M KOH	10	-	234	20
O-CoMoS	1 M KOH	10	2	272	21
A-$CoMoO_4$	1 M KOH	10	1	264	22
CoMoS-PANI	1 M KOH	10	5	250	23
$Co_5Mo_{10}S_x$/CC	1 M KOH	10	2	153	24
CoP(MoP)-$CoMoO_3$@CN	1 M KOH	10	10	296	25
Cu-$Co(OH)_2$	1 M KOH	10	5	300	26
V_P-Fe-CoP	1 M KOH	10	5	300	27
CuMoS	1 M KOH	10	2	270	28
CuMoP	1 M KOH	10	2	213	28
CoMo/CoMoP/NF	1 M KOH	10	5	246	29
CC/MOF-$CoSe_2$@$MoSe_2$	1 M KOH	10	10	183.81	30

Table S2. Comparison of C_{dl}, ECSA and roughness factor (RF) values.

Electrocatalyst	**Slope**	**C_{dl} (mF cm^{-2})**	**ECSA (cm^2)**	**RF**
CuCoMo-LDH	13	6.5	162.5	162.5
CuCoMo-P	35.2	17.6	440	440
CuCoMo-S	6.4	3.2	80	80
$Co(OH)_2$	2.66	1.33	33.25	33.25
CoMo-LDH	5.52	2.76	69	69

CuCo-OH	3.4	1.7	42.5	42.5

Table S3. Solution (R_s), and charge transfer resistance (R_{ct}) obtained from Nyquist plots in the OER region at 1.53 V (vs. RHE).

Electrocatalyst	$\boldsymbol{R_s}$ **(Ω)**	$\boldsymbol{R_{ct}}$ **(Ω)**
CuCoMo-LDH	0.7674	0.4683
CuCoMo-P	0.5563	0.2503
CuCoMo-S	0.8034	0.2964
Bare NF	0.8578	6.381
RuO_2	0.6367	2.961

4. Calculations of exchange current density (j_0):

For CuCoMo-LDH for OER-

$$j_0 = \frac{(8.314\ \text{J K}^{-1}\ \text{mol}^{-1} \times 298\ \text{K})}{(4 \times 96485\ \text{C mol}^{-1} \times 0.4683\ \Omega \times 1\ \text{cm}^2)}$$

$$j_0 = 13.71\ \text{mA cm}^{-2}$$

For CuCoMo-LDH for OER-

$$j_0 = \frac{(8.314\ \text{J K}^{-1}\ \text{mol}^{-1} \times 298\ \text{K})}{(2 \times 96485\ \text{C mol}^{-1} \times 10.04\ \Omega \times 1\ \text{cm}^2)}$$

$$j_0 = 1.28\ \text{mA cm}^{-2}$$

Similarly, all j_0 values were calculated, and presented in **Table S4**.

Table S4. Exchange current densities (j_0) of the electrocatalyst materials.

Electrocatalysts	j_0 for OER (mA cm^{-2})	j_0 for HER (mA cm^{-2})
CuCoMo-LDH	13.71	1.28
CuCoMo-P	25.65	7.97
CuCoMo-S	21.65	0.26

5. Calculation of turnover frequency (TOF) values:

Area under the oxidation curve of CuCoMo-LDH (**Fig. S13a**) = 0.35375 mA V

Hence charge, $\mathrm{Q} = \frac{1}{v}\int_{\mathrm{E_1}}^{\mathrm{E_2}} \mathrm{i(E)\ dE} = \frac{(0.35374\ mA\ V)}{(0.002\ V\ s^{-1})} = 176.87\ \mathrm{mA}\ s^{-1} = 0.17687\ \mathrm{C}$

where v is scan rate in V s^{-1}.

Considering the number of electrons involved is equal to the number of active sites (G),

Number of electrons involved $= \frac{0.17687\ \mathrm{C}}{1.602\times10^{-19}\ \mathrm{C}} = 1.104\times10^{18} = G$

The number of active sites for other electrocatalysts was calculated similarly. The TOF was calculated from the integrated OER LSV curves at a scan rate of 2 mV s^{-1} using equation (8) and shown in **Fig. S13d**.

Table S5. Number of active sites and TOF of the electrocatalysts.

Electrocatalysts	Number of active sites	Potential (V vs. RHE)	TOF (s^{-1})
CuCoMo-LDH	1.104×10^{18}	1.7	0.304
		2.0	0.818
CuCoMo-P	1.617×10^{17}	1.7	1.977
		2.0	6.204
CuCoMo-S	2.053×10^{18}	1.7	0.144
		2.0	0.402

Table S6. Comparison of HER performance of the reported electrocatalysts with recent results.

Electrocatalyst	Electrolyte	Current density ($mA\ cm^{-2}$)	Scan rate ($mV\ s^{-1}$)	Potential (mV. vs RHE)	Ref.
CuCoMo-LDH	1 M KOH	-10	2	79	This work
		-15		111	
		-50		215	
		-100		278	
CuCoMo-P	1 M KOH	-15	2	45	This work
		-50		117	
		-100		190	
CuCoMo-S	1 M KOH	-10	2	167	

		-50 -100		265 333	This work
NiIrSAA-NiFe-LDH	1 M KOH	-10	1	28.5	9
CoMoNiPi	1 M KOH	-10	2	96	18
MoP/$CoMoP_2$@NPC	1 M KOH	-10	5	93	19
MoP/$CoMoP_2$@NPC	0.5 M H_2SO_4	-10	5	71	19
MoP@NPC	0.5 M H_2SO_4	-10 -100	5	109 200	19
$CoMoP_2$@NPC	0.5 M H_2SO_4	-10 -100	5	184 350	19
Mo–$Co(OH)_2/Co_3O_4$/NF-800	1 M KOH	-10	-	116	20
O-CoMoS	1 M KOH	-10	2	97	21
CoMoS-PANI	1 M KOH	-10	5	98	23
$Co_5Mo_{10}S_x$/CC	1 M KOH	-10	2	36	24
CoP(MoP)-$CoMoO_3$@CN	1 M KOH	-10	10	198	25
V_P-Fe-CoP	1 M KOH	-10	5	143	27
CuMoS	1 M KOH	-10	2	207	28
CuMoP	1 M KOH	-10	2	147	28
CoMo/CoMoP/NF	1 M KOH	-10	5	29	29
CC/MOF-$CoSe_2$@$MoSe_2$	1 M KOH	10	10	109.87	30

Table S7. Solution (R_s), and charge transfer resistance (R_{ct}) obtained from Nyquist plots in the HER region at -0.075 V (vs. RHE).

Electrocatalyst	R_s (Ω)	R_{ct} (Ω)
CuCoMo-LDH	0.407	10.04
CuCoMo-P	0.769	1.61
CuCoMo-S	0.850	47.66

Table S8. Comparison of OWS performance of the reported electrocatalysts with recent results.

Anode Electrocatalyst	Cathode Electrocatalyst	Electrolyte	Current density (mA cm^{-2})	Scan rate (mV s^{-1})	Cell potential (V)	Ref.
RuO_2	Pt/C (10%)	1 M KOH	10 50 100	2	1.554 1.741 1.898	This work
CuCoMo-LDH	CuCoMo-LDH	1 M KOH	10 50 100	2	1.427 1.732 1.863	This work
CuCoMo-P	CuCoMo-P	1 M KOH	10 50 100	2	1.393 1.633 1.738	This work
CuCoMo-S	CuCoMo-S	1 M KOH	10	2	1.540	

			15 50 100		1.599 1.818 1.970	This work
IrSAC-NiFe-LDH	NiIrSAA-NiFe-LDH	1 M KOH	10	1	1.49	9
CoMoNiPi	CoMoNiPi	1 M KOH	10 100	2	1.59 1.9	18
MoP/$CoMoP_2$@NPC	MoP/$CoMoP_2$@NPC	0.5 M H_2SO_4	10	5	1.52	19
MoP/$CoMoP_2$@NPC	MoP/$CoMoP_2$@NPC	1 M KOH	10	5	1.53	19
Mo–$Co(OH)_2/Co_3O_4$/NF-800	Mo–$Co(OH)_2/Co_3O_4$/NF-800	1 M KOH	10	-	1.62	20
O-CoMoS	O-CoMoS	1 M KOH	10	2	1.60	21
A-$CoMoO_4$	A-$CoMoO_4$	1 M KOH	10	1	1.51	22
CoMoS-PANI	CoMoS-PANI	1 M KOH	10	5	1.58	23
$Co_5Mo_{10}S_x$/CC	$Co_5Mo_{10}S_x$/CC	1 M KOH	10 100	2	1.51 1.78	24
CoP(MoP)-$CoMoO_3$@CN	CoP(MoP)-$CoMoO_3$@CN	1 M KOH	10	10	1.55	25
V_P-Fe-CoP	V_P-Fe-CoP	1 M KOH	10	5	1.63	27
CoMo/CoMoP	CoMo/CoMoP	1 M KOH	10	5	1.54	29
CC/MOF-$CoSe_2$@$MoSe_2$	CC/MOF-$CoSe_2$@$MoSe_2$	1 M KOH	10	10	1.53	30

a-$CoMoO_3$	a-$CoMoO_3$	1 M KOH	10	2	1.5	31

References

1 G. Rajeshkhanna, T. I. Singh, N. H. Kim and J. H. Lee, *ACS Appl. Mater. Interfaces*, 2018, **10**, 42453.

2 S. Shit, S. Chhetri, W. Jang, N. C. Murmu, H. Koo, P. Samanta and T. Kuila, *ACS Appl. Mater. Interfaces*, 2018, **10**, 27712.

3 M. Yu, E. Budiyanto and H. Tüysüz, *Angew. Chem. Int. Ed.*, 2022, **61**, e202103824.

4 A. Borah, Sumit, S. Palaniyappan and G. Rajeshkhanna, *Sustain. Energy Fuels*, 2024, **8**, 2265.

5 D. Wang, J. Wang, X. Luo, Z. Wu and L. Ye, *ACS Sustain. Chem. Eng.*, 2018, **6**, 983.

6 G. A. Gebreslase, M. V. Martínez-Huerta and M. J. Lázaro, *J. Energy Chem.*, 2022, **67**, 101.

7 H. Liu, Z. Guo, Q. Zhang, B. Jin and R. Peng, *ACS Omega*, 2021, **6**, 25440.

8 T. U. Haq, S. A. Mansour, A. Munir and Y. Haik, *Adv. Funct. Mater.*, 2020, **30**, 1910309.

9 Y. Hu, T. Shen, Z. Song, Z. Wu, S. Bai, G. Liu, X. Sun, Y. Wang, S. Hu, L. Zheng and Y. F. Song, *ACS Catal.*, 2023, **13**, 11195.

10 G. Kresse and J. Furthmü, *Phys. Rev. B*, 1996, **54**, 11169.

11 J. P. Perdew, K. Burke and M. Ernzerhof, *Phys. Rev. Lett.*, 1996, **77**, 3865.

12 P. E. Blochl, *Phys. Rev. B*, 1994, **50**, 17953.

13 L. S. Pedroza, A. J. R. Da Silva and K. Capelle, *Phys. Rev. B*, 2009, **79**, 201106.

14 J. P. Perdew, A. Ruzsinszky, G. I. Csonka, O. A. Vydrov, G. E. Scuseria, L. A. Constantin, X. Zhou and K. Burke, *Phys. Rev. Lett.*, 2008, **100**, 136406.

15 G. Kresse and J. Furthmiiller, *Comput. Mater. Sci.*, 1996**, 6**, 15.

16 H. J. Monkhorst and J. D. Pack, *Phys. Rev. B*, 1976, **13**, 5188.

17 J. K. Nørskov, J. Rossmeisl, A. Logadottir, L. Lindqvist, J. R. Kitchin, T. Bligaard and H. Jónsson, *J. Phys. Chem. B*, 2004, **108**, 17886.

18 P. Viswanathan and K. Kim, *ACS Appl. Mater. Interfaces*, 2023, **15**, 16571.

19 L. Zheng, C. Liu, W. Zhang, B. Gao, T. Yan, Y. Zhang, X. Cao, Q. Gao and Y. Tang, *J. Mater. Chem. A*, 2024, **12**, 1243.

20 H. Yang, T. Hu, R. Meng and L. Guo, *J. Solid State Chem.*, 2023, **320**, 123837.

21 J. Hou, B. Zhang, Z. Li, S. Cao, Y. Sun, Y. Wu, Z. Gao and L. Sun, *ACS Catal.*, 2018, **8**, 4612.

22 L. Ge, W. Lai, Y. Deng, J. Bao, B. Ouyang and H. Li, *Inorg. Chem.*, 2022, **61**, 2619.

23 S. Mathew, J. H. Sim, R. Rajmohan, O. L. Li and Y. R. Cho, *Electrochim. Acta*, 2022, **403**, 139586.

24 Y. Lu, X. Guo, L. Yang, W. Yang, W. Sun, Y. Tuo, Y. Zhou, S. Wang, Y. Pan, W. Yan, D. Sun and Y. Liu, *Chem. Eng. J.*, 2020, **394**, 124849.

25 L. Yu, Y. Xiao, C. Luan, J. Yang, H. Qiao, Y. Wang, X. Zhang, X. Dai, Y. Yang and H. Zhao, *ACS Appl. Mater. Interfaces*, 2019, **11**, 6890.

26 L. Chen, H. Zhang, L. Chen, X. Wei, J. Shi and M. He, *J. Mater. Chem. A*, 2017, **5**, 22568.

27 R. Na, K. Min, M. Kim, S. Min and S. H. Baeck, *Adv. Sustain. Syst.*, 2023, **7**, 2300130.

28 J. Choi, K. Morey, A. Kumar, D. Neupane, S. R. Mishra, F. Perez and R. K. Gupta, *Mater. Today Chem.*, 2022, **24**, 100848.

29 Y. Lu, X. Zheng, Y. Liu, J. Zhu, D. Li and D. Jiang, *Inorg. Chem.*, 2022, **61**, 8328.

30 S. J. Patil, N. R. Chodankar, S. K. Hwang, P. A. Shinde, S. R. G. Raju, S. K. Ranjith, Y. S. Huh and Y. K. Han, *Chem. Eng. J.*, 2022, **429**, 132379.

31 E. Hu, Y. Yao, Y. Chen, Y. Cui, Z. Wang and G. Qian, *ACS Appl. Energy. Mater.*, 2021, **4**, 6740.